Electronic Supplementary information

Hexagonal 2D covalent organic frameworks from nonpolar and symmetric electron-absorbing substituents for electron transport layers in near-infrared PeLEDs

Lili Xu,[a] Lei Zheng,[a] Yu Jing,[b] Xiangyu Guo,[c] Xuemin Hu,[*d] Bo Xu,[a] and Shengli Zhang[*a]

[a.] MIIT Key Laboratory of Advanced Display Materials and Devices, School of Materials Science and Engineering, Nanjing University of Science and Technology, Nanjing 210094, Jiangsu, China; E-mail: zhangslvip@njust.edu.cn

[b.] Jiangsu Co-Innovation Centre of Efficient Processing and Utilization of Forest Resources College of Chemical Engineering, Nanjing Forestry University, Nanjing 210037, China

[c.] School of Science, Constructor University, Bremen 28759, Germany.

[d.] School of Material Engineering, Jinling Institute of Technology, Nanjing 211169, China; E-mail: huxuemvip@126.com

Table of Contents

3. Supplementary Tables

Table S1. Full names of 23 linear diamine linkers.

Table S2. Lattice constants, valence band maximums (VBM), conduction band minimums (CBM), band gaps (Gap), and work functions (WF) of 23 β-ketoenamine linked 2D COFs by PBE functional.

Table S3. Lattice parameters of sp^2 carbon conjugated 2D COFs.

Table S4. Valence band maximums (VBMs), conduction band minimums (CBMs), and band gaps of 2D COFs with different substituents in 2D Tp-DAAQ by HSE06 functional.

4. Supplementary References

1. Calculation Details

VASP: All calculations are performed using a cut-off energy of 400 eV with the 2 × 2 × 1 Monkhorst-Pack grid. The calculations are stopped until the force less than 0.01 eV/Å, and the energy convergence criterion is set to 10^{-6} eV. The vacuum is separated by 20 Å along the z-direction to prevent interaction between periodic structures.

PWmat: The SG15 norm-conserving pseudopotentials[1] are applied with an energy cutoff of 50 Ry. Optimization and electronic property calculations are performed using a 2 × 2 × 1 Monkhorst-Pack grid.

Hefei-NAMD: Firstly, the program heats up to 300K. Secondly, after system equilibration, an adiabatic molecular dynamics trajectory of 5 ps is obtained. Extract snapshots from the MD traces and perform Self-Consistent Field (SCF) calculations for each snapshot. Finally, read the WAVECAR from SCF to perform the NAMD calculation. Specifically, NAMD calculation is performed using the quantum classical dephasing induced surface hopping (DISH) method under the classical path approximation. The 4 ps non-adiabatic Hamiltonian is iterated 500 times to calculate the e-h recombination process on nanosecond time scales. The NAMD result is based on the average of 50 randomly sampled initial structures. The software has been widely used in the study of carrier dynamics.[2-5]

Heterojunction: In order to make the lattice mismatch less than 6%, we applied an uniaxial stress of 6% in the b direction to the 2D COF and constructed a heterojunction with a 6 × 3 × 1 $CsPbI_3$ layer on the (001) face and a 1 × 1 monolayer 2D Tp-DABDA. $CsPbI_3$ (001) is modeled as a five-layer slab, and the bottom two layers are fixed. Although the HSE06 and spin-orbit coupling (SOC) fully takes into account the influence of lead atoms, the HSE06+SOC calculation is bound to be resource-intensive due to the large number of atoms in $CsPbI_3$/Tp-DABDA (426 atoms). Therefore, we mainly use PBE functional for the analysis of heterojunctions, and the conclusions can already qualitatively illustrate the trend of the electronic structure changes at the interface. The DFT-D3 vdW correction and dipole correction are considered in all calculations.

To demonstrate its stability, we calculated the binding energy E_{bin}, which is given by $E_{bin} = E_{total} - E_{CsPbI3} - E_{Tp\text{-}DABDA}$, E_{total} refers to the total energy of the heterojunction, E_{CsPbI3} and $E_{Tp\text{-}DABDA}$ are the energies of $CsPbI_3$ and 2D Tp-DABDA layers, respectively. The more negative E_{bin} is, the more stable the interface is. The calculated result shows a binding energy of −1.22 eV, which proves that 2D Tp-DABDA/$CsPbI_3$ is stable. To demonstrate the thermodynamic stability, the electron localization function (ELF) is used to analyze the chemical bonding at the heterojunction interface. It can be seen from Fig. S14a that $CsPbI_3$ is ionically bonded to 2D Tp-DABDA. The charge will be redistributed when the EML forms an interface with the ETL. Accordingly, we observe the effect of the interface structure on the carrier separation and transport processes by analyzing the deformation charge density (DCD). As can be seen in Fig. S14b, $CsPbI_3$ is in the charge accumulation region, while the 2D Tp-DABDA layer is the charge depletion region.

The driving force for photogenerated carrier separation and transport is influenced by the electrostatic potential difference between the EML and ETL. In the end, we calculated the electrostatic potential of the 2D Tp-DABDA/$CsPbI_3$ interface in the z-direction, as shown in Fig. S14c. The calculation demonstrates that there is a potential difference at the 2D Tp-DABDA/$CsPbI_3$ interface, which can increase the charge transfer driving force. To more accurately represent the electron injection efficiency, the tunneling probability can be calculated:[6]

$$T_{TB} = \exp\left(- 2\frac{\sqrt{2m\Phi_{TB}}}{\hbar} \times W_{TB} \right)$$

where m and ħ are the free electron mass and Planck constant, Φ_{TB} is the height of the tunneling barrier, and W_{TB} is the width of the tunneling barrier respectively. Generally, a comprehensive factor $C = W_{TB}\sqrt{\Phi_{TB}}$ is proposed to evaluate the tunneling potential barrier to simplify the calculation. The results are shown in Fig. S14c, Φ_{TB} is 4.1 eV.

2. Supplementary Figures

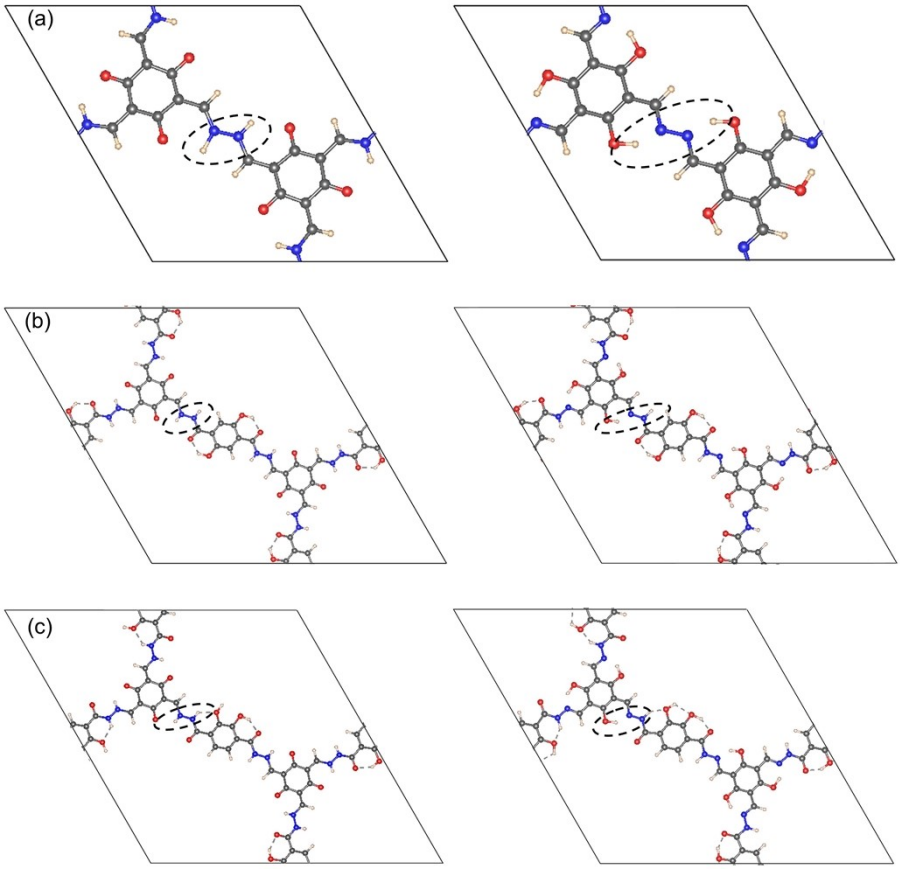

Fig. S1. Schematic diagram of the hydrazone-linked 2D COF structures of (a) Azine-Triformylphloroglucinol-COF (ATFG-COF), and hydrazone-based COFs (b) NUS-50 and (c) NUS-51 before (left panel) and after (right panel) optimization.

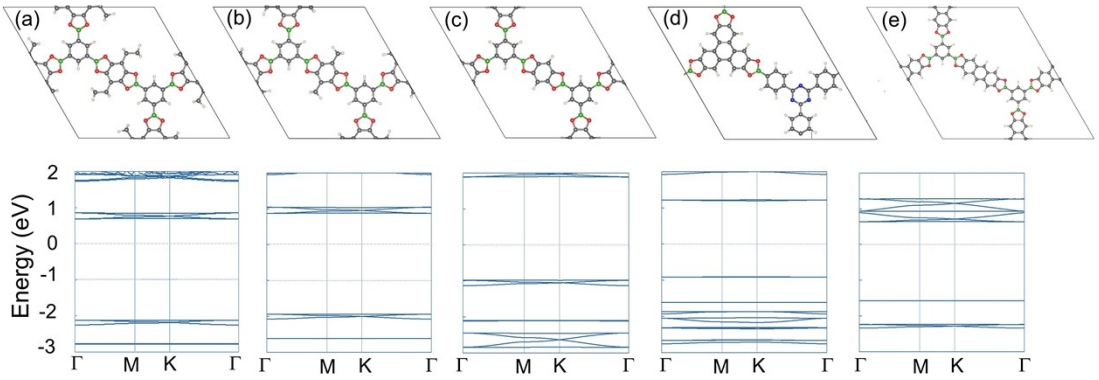

Fig. S2. Boronate anhydride-based 2D COFs of (a) COF-14Å, (b) COF-16Å, (c) COF-18Å, (d) BTA-COF1, and (e) Ph-An-COF.

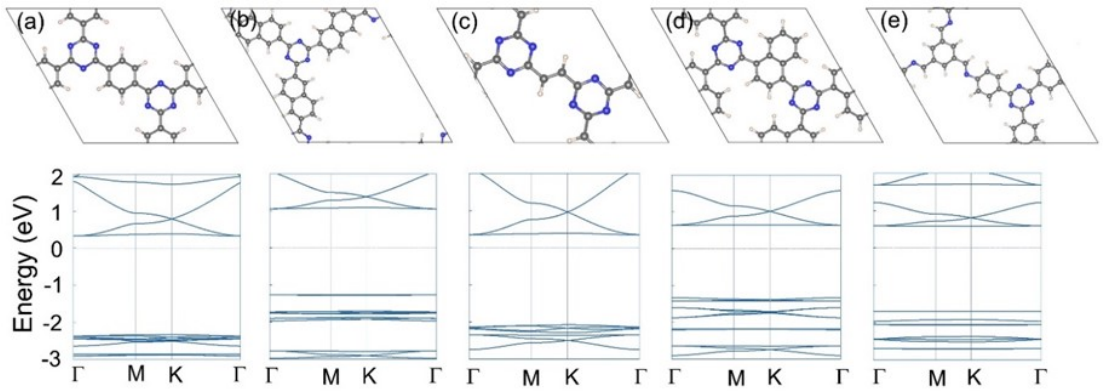

Fig. S3. Nitrile-based 2D COFs of (a) CTF-1, (b) CTF-2-B-I, (c) CTF-FUM, (d) CTF-DCN, and (e) PI-3-COF.

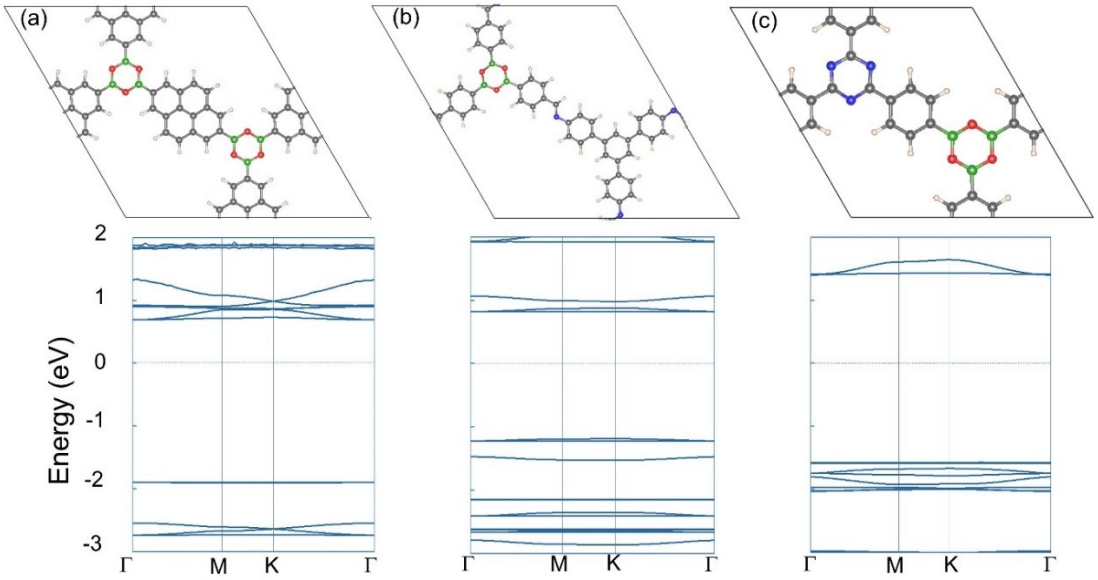

Fig. S4. Boronate ester-based 2D COFs of (a) PPy-COF, (b) NTU-COF-1, and (c) TB-COF.

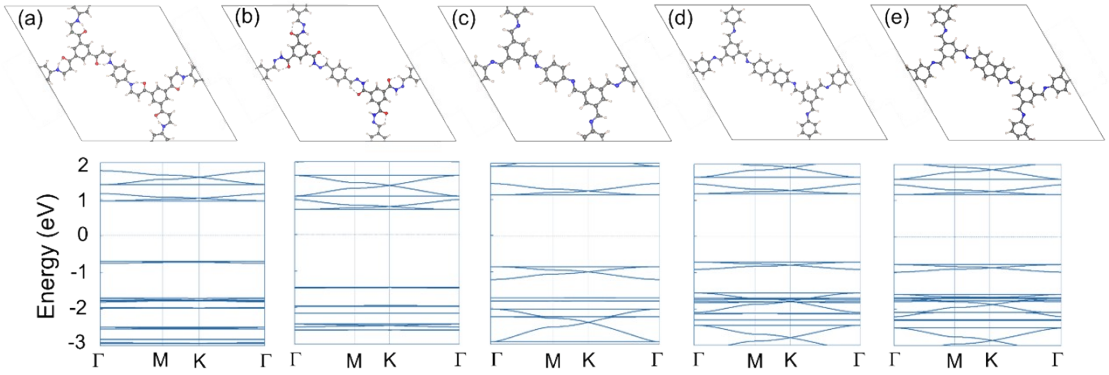

Fig. S5. Imine-based 2D COFs of (a) COF-3PD, (b) COF-ASB, (c) COF-LZU1, (d) BND-TFP COF, and (e) FL-COF-1.

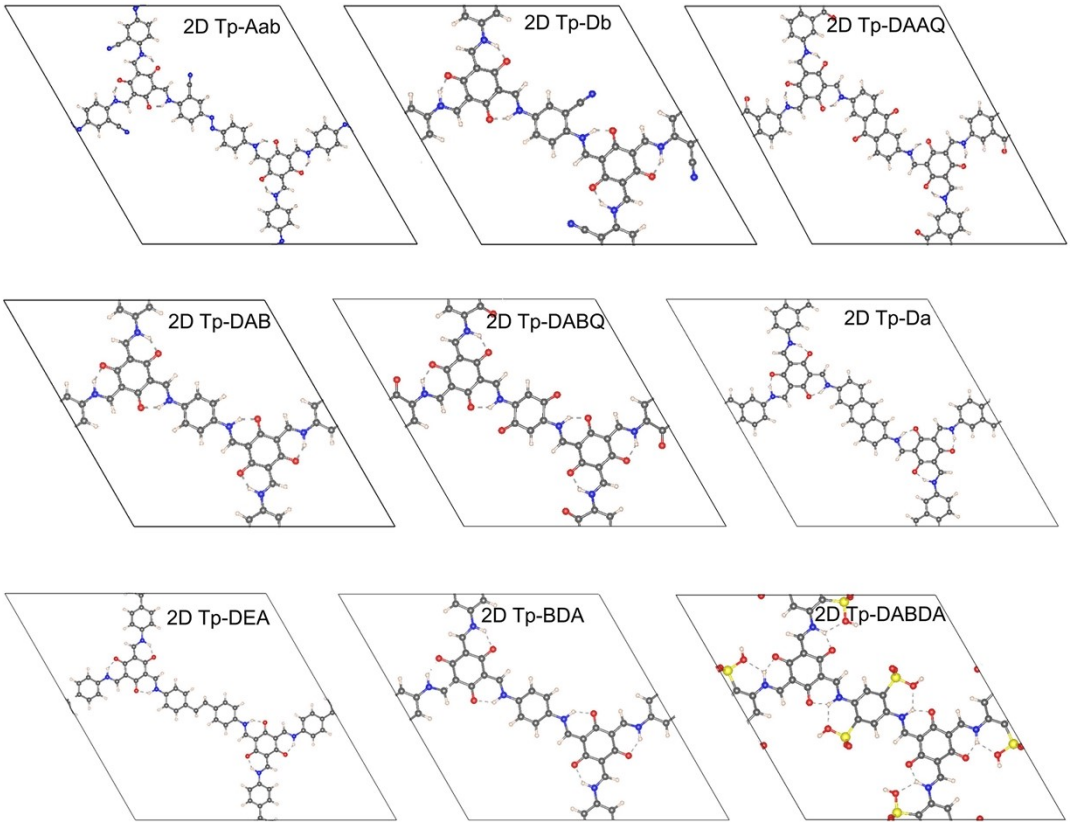

Fig. S6. Structure diagrams of β-ketoenamine linked 2D COFs.

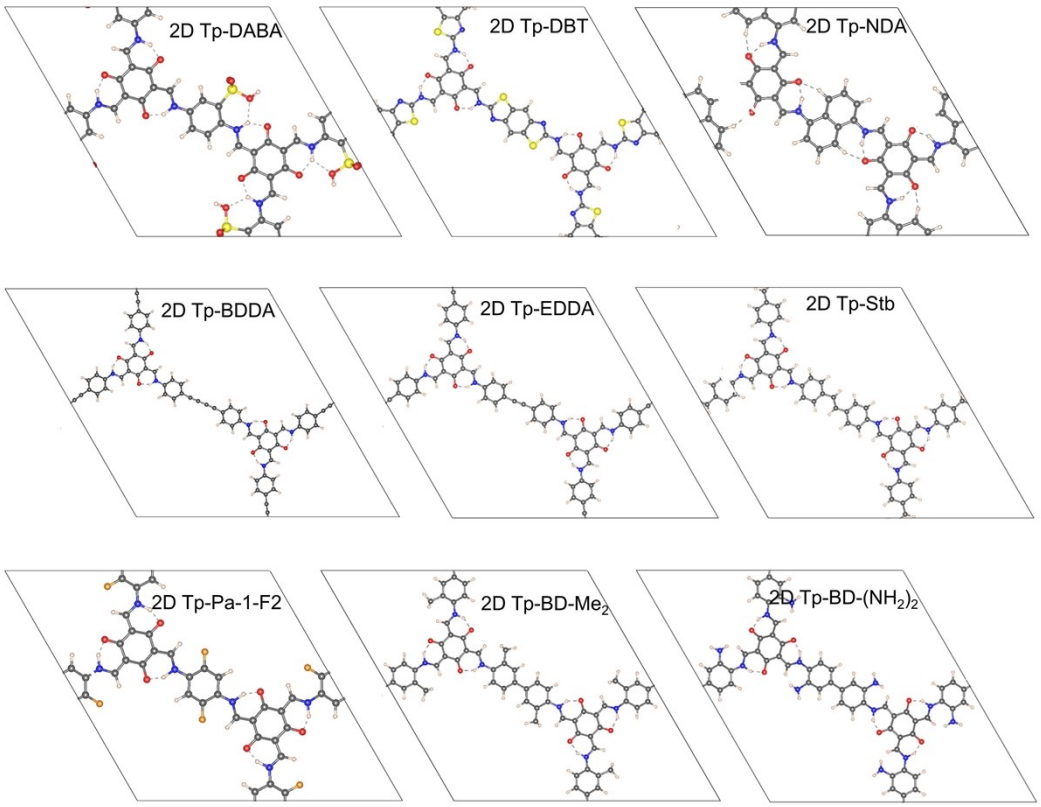

Fig. S7. Structure diagrams of β-ketoenamine linked 2D COFs.

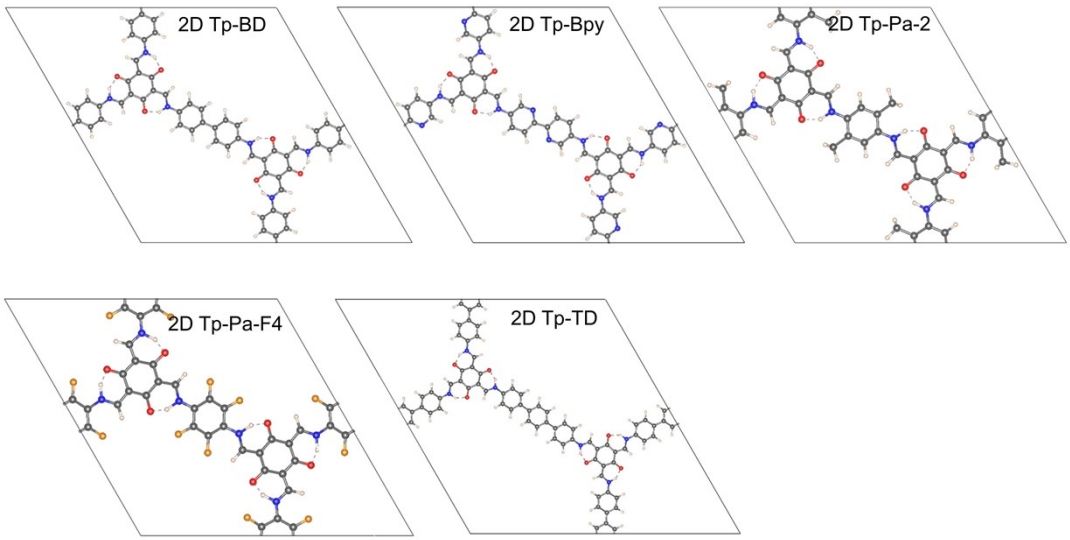

Fig. S8. Structure diagrams of β-ketoenamine linked 2D COFs.

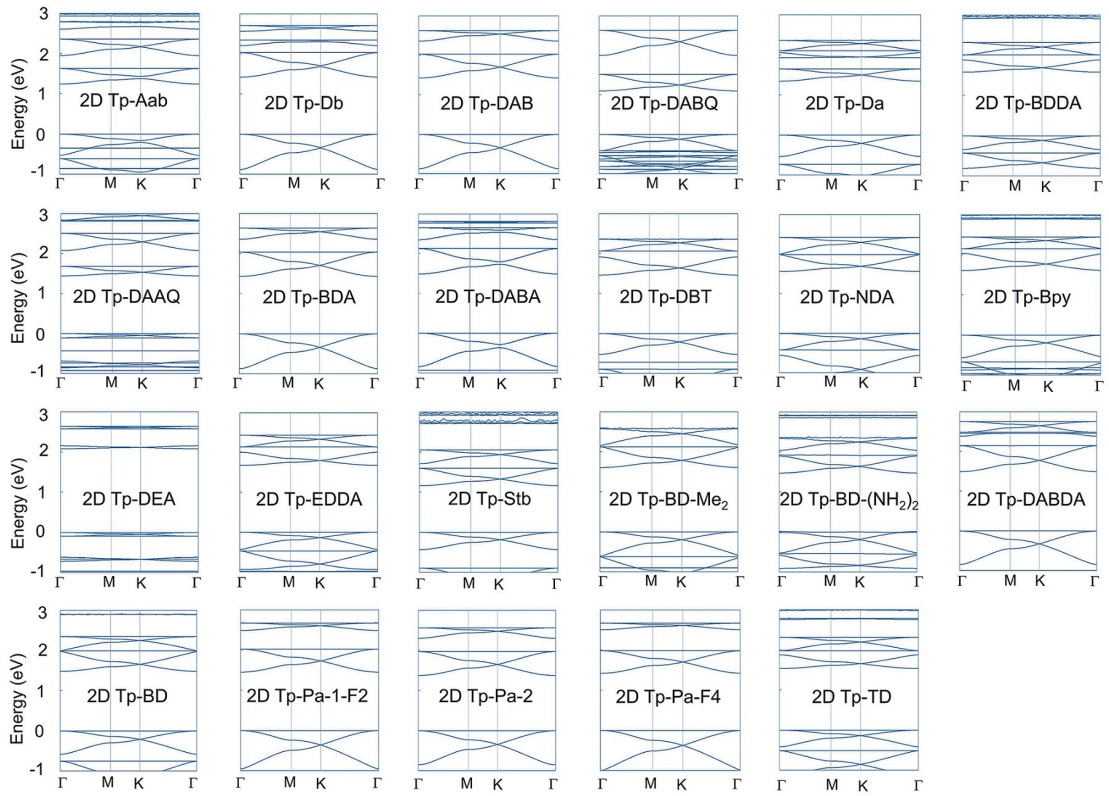

Fig. S9. Band structures of β-ketoenamine linked 2D COFs by using PBE functional. VBM is set to zero.

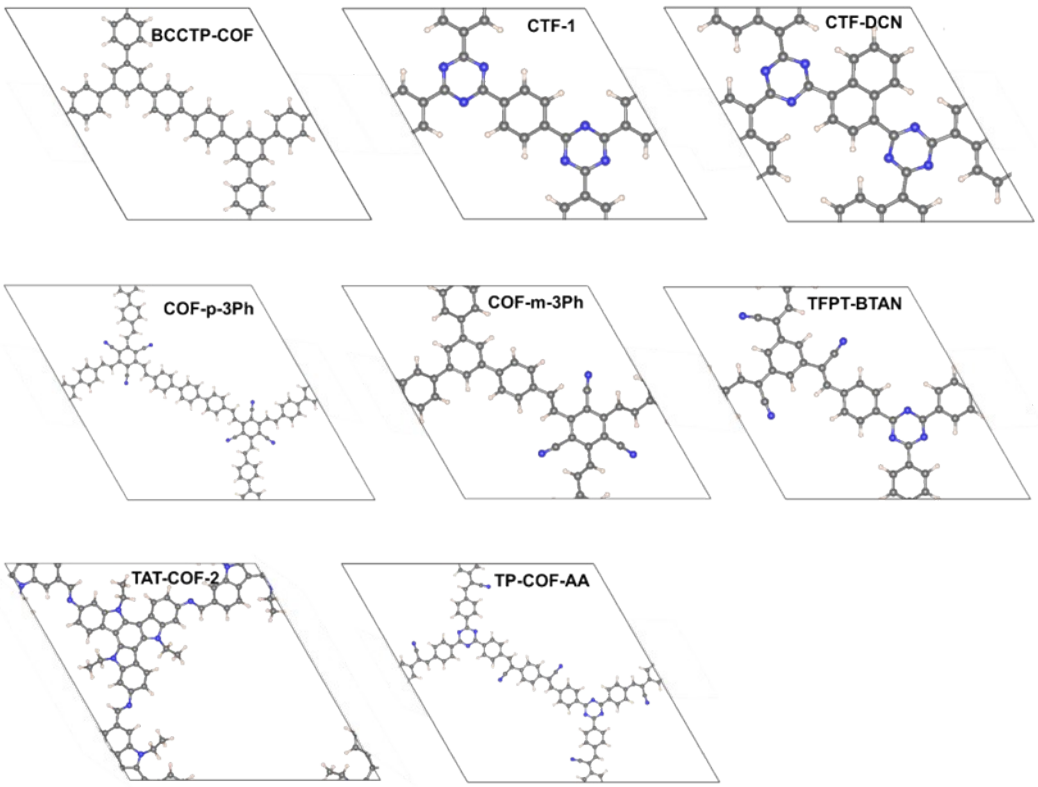

Fig. S10. Structures of sp^2 carbon conjugated 2D COFs.

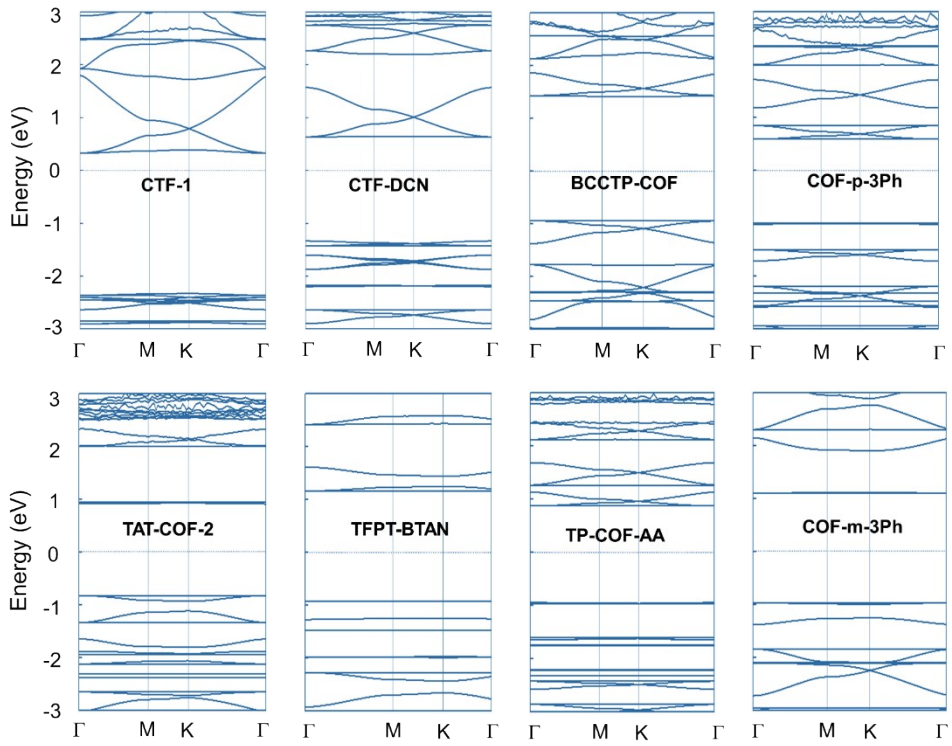

Fig. S11. Band structures of sp^2 carbon conjugated 2D COFs.

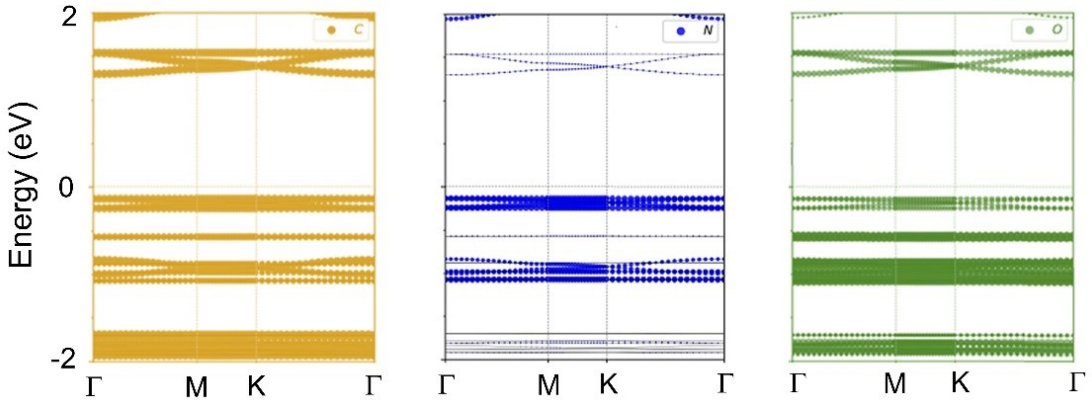

Fig. S12. Projected band structure of 2D Tp-DAAQ.

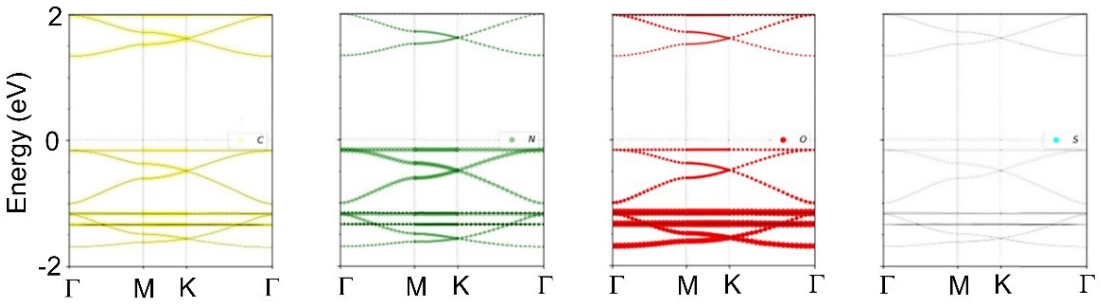

Fig. S13. Projected band structure of 2D Tp-DABDA.

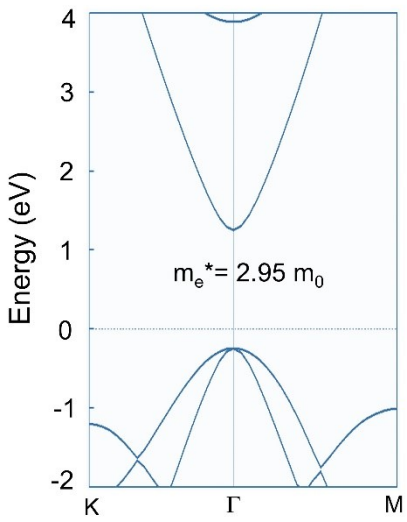

Fig. S14. Energy band structure and corresponding electron effective mass of monolayer ZnO.

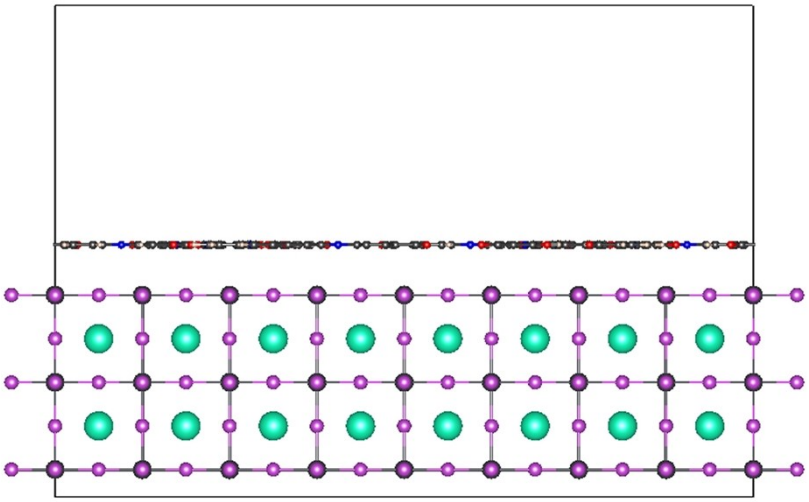

Fig. S15. Schematic diagram of 2D Tp-DAAQ/$CsPbI_3$ heterojunction.

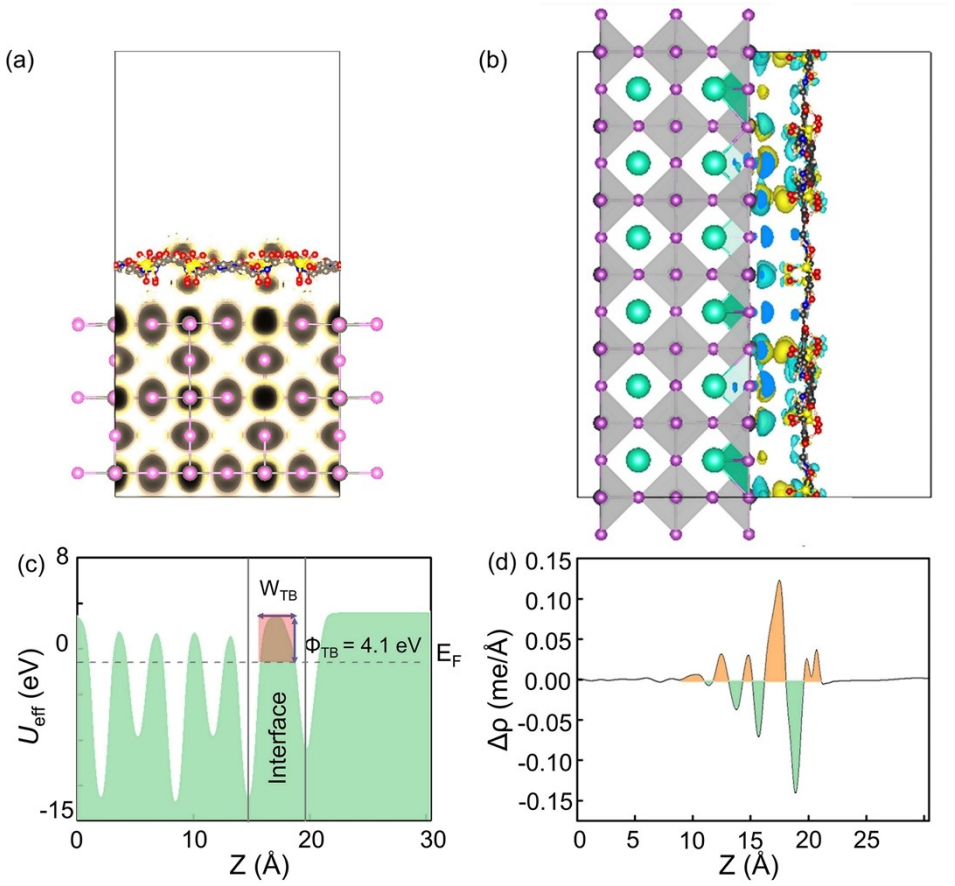

Fig. S16. (a) Electron localization function (ELF), (b) deformation charge density (DCD), (c) electrostatic potential in 2D Tp-DABDA/$CsPbI_3$, and (d) planar-averaged differential charge density along z direction for 2D Tp-DABDA/$CsPbI_3$ heterojunction.

3. Supplementary Tables

Table S1. Full names of 23 linear diamine linkers.

Aab	2-amino-5-((4-aminophenyl)diazenyl)benzonitrile
Db	2,5-diaminobenzonitrile
DAAQ	2,6-diaminoanthraquinone
DAB	p-diaminobenzene
DABQ	2,5-diamino 1,4-benzoquinone
Da	2,6-diaminoanthracene
DEA	4,4'-ethylenedianiline
BDA	benzene-1,4-diamine
DABDA	2,5-diaminobenzene1,4-disulfonic acid
DABA	2,5-diaminobenzenesulfonic acid
DBT	2,6-diaminobenzo[1,2-d:4,5-d′]bisthiazole
NDA	1,5-diaminonaphthalene
BDDA	4,4'-(buta-1,3-diyne-1,4-diyl)dianiline)
DANT	2,7-diaminobenzo[lmn][3,8]phenanthroline-1,3,6,8(2H,7H) tetraone
EDDA	4,4'-(ethyne-1,2-diyl)dianiline
Stb	4,4'-diaminostilbene
BD-Me_2	o-tolidine
BD-$(NH_2)_2$	3,3'-diaminobenzidine
BD	benzidine
Bpy	2,20-bipyridine-5,50-diamine
Pa-1-F2	p-phenylenediamine-F2
Pa-2	2,5-dimethyl-p-phenylenediamine
Pa-F4	2,3,5,6-tetrafluoro-1,4-phenylenediamine
TD	4,4''-Diamino-p-terphenyl

Table S2. Lattice constants, valence band maximums (VBM), conduction band minimums (CBM), band gaps (Gap), and work functions (WF) of 23 β-ketoenamine linked 2D COFs by PBE functional.

Species	Lattice constants (Å)	VBM (eV)	CBM (eV)	Gap (eV)	WF (eV)
2D Tp-Aab	a=b=32.54	-5.31	-4.07	1.24	4.61
2D Tp-Db	a=b=21.56	-5.20	-3.78	1.42	4.51
2D Tp-DAB	a=b=21.73	-4.89	-3.47	1.42	4.07
2D Tp-DABQ	a=b=21.51	-6.10	-5.0	1.10	5.53
2D Tp-Da	a=b=28.77	-4.58	-3.24	1.34	3.94
2D Tp-DAAQ	a=b=28.64	-5.61	-4.16	1.45	4.92
2D Tp-BDA	a=b=22.55	-4.89	-3.46	1.43	4.09
2D Tp-DABDA	a=b=21.42	-5.69	-4.19	1.50	4.71
2D Tp-DABA	a=b=21.59	-5.27	-3.78	1.49	4.61
2D Tp-DBT	a=b=28.53	-5.29	-3.83	1.46	4.69
2D Tp-NDA	a=b=22.02	-4.98	-3.42	1.56	4.04
2D Tp-BDDA	a=b=37.71	-4.93	-3.35	1.58	4.18
2D Tp-EDDA	a=b=33.29	-4.89	-3.21	1.68	3.85
2D Tp-Stb	a=b=32.01	-4.39	-3.23	1.16	3.77
2D Tp-BD-Me_2	a=b=29.81	-4.73	-3.12	1.61	3.73
2D Tp-BD-$(NH_2)_2$	a=b=28.72	-4.36	-2.90	1.46	3.53
2D Tp-BD	a=b=28.87	-4.72	-3.24	1.48	3.87
2D Tp-Pa-1-F2	a=b=21.55	-4.95	-3.50	1.45	4.30
2D Tp-Pa-2	a=b=21.68	-4.80	-3.43	1.37	4.03
2D Tp-Pa-F4	a=b=21.28	-5.07	-3.65	1.42	4.29
2D Tp-TD	a=b=36.55	-4.74	-3.20	1.54	4.04
2D Tp-DEA	a=b=32.65	-4.99	-2.91	2.08	4.22
2D Tp-Bpy	a=b=28.47	-5.19	-3.58	1.61	4.12

Table S3. Lattice parameters of sp^2 carbon conjugated 2D COFs.

2D COFs	Lattice constants (Å)	Reference
BCCTP-COF	a=b=22.38	7
CTF-1	a=b= 14.32	8
CTF-DCN	a=b= 14.48	9
COF-*p*-3Ph	a=b= 37.61	10
COF-*m*-3Ph	a=b=18.55	10
TAT-COF-2	a=b= 24.68	11
TFPT-BTAN	a=b= 18.58	12
TP-COF-AA	a=b= 36.78	13

Table S4. Valence band maximums (VBMs), conduction band minimums (CBMs), and band gaps of 2D COFs with different substituents in 2D Tp-DAAQ by HSE06 functional.

Species	Substitution	VBM (eV)	CBM (eV)	Gap (eV)
2D Tp-DAAQ	−H	-4.89	-3.03	1.86
2D Tp-DAAQ	−OH	-4.63	-2.95	1.68
2D Tp-DAAQ	$-CH_3$	-4.78	-2.93	1.85
2D Tp-DAAQ	−CN	-5.49	-3.98	1.51
2D Tp-DAAQ	$-NO_2$	-5.65	-4.04	1.61
2D Tp-DAAQ	−F	-4.95	-3.19	1.76

4. Supplementary References

1 D. R. Hamann, *Phys. Rev. B*, 2013, **88**, 085117.

2 W. Chu, Q. Zheng, O. V. Prezhdo, J. Zhao, W. A. Saidi, *Sci. Adv.*, 2020, **6**, eaaw7453.

3 X. Jiang, Q. Zheng; Z. Lan, W. A. Saidi, X. Ren, J. Zhao, *Sci. Adv.*, 2021, **7**, eabf3759.

4 W. Chu, Q. Zheng, O. V. Prezhdo, J. Zhao, *J. Am. Chem. Soc.*, 2020, **142**, 3214-3221.

5 K. Ni, J. Du, J. Yang, S. Xu, X. Cong, N. Shu, K. Zhang, A. Wang, F. Wang, L. Ge, J. Zhao, Y. Qu, K. S. Novoselov, P. Tan, F. Su, Y. Zhu, *Phys. Rev. Lett.*, 2021, **126**, 027402.

6 Y. Wang, R. X. Yang, R. Quhe, H. Zhong, L. Cong, M. Ye, Z. Ni, Z. Song, J. Yang, J. Shi, J. Li, J. Lu, *Nanoscale*, 2016, **8**, 1179-1191.

7. K. J. Shi, X. Zhang, C. H. Shu, D. Y. Li, X. Y. Wu and P. N. Liu, *Chem. Commun*., 2016, **52**, 8726-8729.

8. P. Kuhn, M. Antonietti and A. Thomas, *Angew. Chem. Int. Ed.*, 2008, **47**, 3450-3453.

9. K. Wang, H. Huang, D. Liu, C. Wang, J. Li and C. Zhong, *Environmental Science & Technology*, 2016, **50**, 4869-4876.

10. S. Bi, P. Thiruvengadam, S. Wei, W. Zhang, F. Zhang, L. Gao, J. Xu, D. Wu, J.-S. Chen and F. Zhang, *J. Am. Chem. Soc.*, 2020, **142**, 11893-11900.

11. Y.-F. Xie, S.-Y. Ding, J.-M. Liu, W. Wang and Q.-Y. Zheng, *J. Mater. Chem. C*, 2015, **3**, 10066-10069.

12. W.-R. Cui, C.-R. Zhang, W. Jiang, F.-F. Li, R.-P. Liang, J. Liu and J.-D. Qiu, *Nat. Commun.*, 2020, **11**, 436.

13. Y. Zhao, H. Liu, C. Wu, Z. Zhang, Q. Pan, F. Hu, R. Wang, P. Li, X. Huang and Z. Li, *Angew. Chem. Int. Ed*., 2019, **58**, 5376-5381.